Contact analyses for anisotropic half-space coated with an anisotropic layer: effect of the anisotropy on the pressure distribution and contact area

Caroline Bagault, Daniel Nelias, Marie-Christine Baietto, Timothy C Ovaert

International Journal of Solids and Structures 50 (2013) 743–754

Contents lists available at SciVerse ScienceDirect

International Journal of Solids and Structures

journal homepage: www.elsevier.com/locate/ijsolstr

Contact analyses for anisotropic half-space coated with an anisotropic layer: Effect of the anisotropy on the pressure distribution and contact area

C. Bagault [a], D. Nélias [a,*], M.C. Baietto [a], T.C. Ovaert [b]

[a] Université de Lyon, CNRS INSA-Lyon, LaMCoS UMR5259, F69621, France
[b] Department of Aerospace and Mechanical Engineering, University of Notre Dame, Notre Dame, IN 46556, United States

ARTICLE INFO

Article history:
Received 24 July 2012
Received in revised form 29 October 2012
Available online 27 November 2012

Keywords:
Contact
Anisotropic
Coating
Analytical solutions
Green function
Half space
Three-dimensional elasticity solution

ABSTRACT

A contact model using semi analytical methods, relying on elementary analytical solutions, has been developed. It is based on numerical techniques adapted to contact mechanics, with strong potential for inelastic, inhomogeneous or anisotropic materials. Recent developments aim to quantify displacements and stresses of a layered anisotropic elastic half space which is in contact with a rigid sphere. The influence of material properties and layer thickness on the contact problem solution will be more specifically analyzed.

1. Introduction

Engineering problems are becoming more complicated when trying to reduce the gap between the model and the actual application. It means that less restrictive assumptions should be made, or in other words more physics should be implemented in the model. Among the challenges to succeed in it, the material properties should be considered accurately. Supposing the material is isotropic is not enough. For most composite and mono-crystal materials their compositions or the elaboration and manufacturing processes imply that it exists one or two main directions or even a general anisotropy. Moreover, coatings are often used to prevent or control wear. Coatings do not have, generally, the same properties than the substrate and may have various thicknesses. The influence of the anisotropy orientations (in the coating and in the substrate) has to be taken into account to better predict the distribution of the contact pressure and the subsurface stress-field in order to optimize the service life of industrial components.

The Green's functions of a point force applied in an isotropic infinite space was first solved by Kelvin (1848). Boussinesq (1885) derived surface Green's functions for a force normal to the free surface, in isotropic solids. Then, Mindlin (1936), by adding a complementary part of the solution, reduced the Kelvin's infinite space functions to the half space Green's functions. Ting and Lee (1997) developed an explicit expression of the Green's functions in terms of the Stroh eigenvalues (Stroh, 1958; Stroh, 1962), for an anisotropic infinite space. Also using the Stroh formalism, Ting (1996) obtained the anisotropic Green's functions of a point force in a half space in the Fourier transformed domain. With inverse fast Fourier transforms, solutions can be finally obtained in the physical domain. The three dimensional Green's functions of point forces were studied in anisotropic bimaterials (Pan and Yuan, 2000), in anisotropic trimaterials (Yang and Pan, 2002) and also at the interface of an anisotropic bimaterial (Pan and Yang, 2003). Ciavarella et al. (2001) presented a method for solving 3D contact problem for anisotropic materials by using the standard Hertzian solution. Li and Wang (2006) worked also with the Hertzian solution in order to analyze the contact problem for two anisotropic piezoelectric bodies pressed together. Borodich (2000) solved some contact problems of anisotropic elastodynamics by applying his method of integral characteristics of solutions to boundary-initial value problems. Swanson (2004) used the procedure outlined by Willis (1966), a numerical contour integration to determine the contact area and the pressure distribution, combined with the Pagano solution (Pagano, 1970) to obtain detailed stress fields. Gao and Pharr (2007) were interested by the effective moduli of elastically anisotropic solids under normal and tangential contacts. In their books, Rand and Rovenskii (2005) focused on the procedure of obtaining analytical solutions in anisotropic elasticity and Galin (2008) dealt with contact problems and got onto contact problems for an anisotropic half plane. Lin and Ovaert (2004) studied the rough surface contact for anisotropic materials

* Corresponding author. Tel.: +33 4 72 43 84 90; fax: +33 4 72 43 89 13.
E-mail address: daniel.nelias@insa-lyon.fr (D. Nélias).

0020-7683/$ - see front matter © 2012 Elsevier Ltd. All rights reserved.
http://dx.doi.org/10.1016/j.ijsolstr.2012.11.002

in 2D. Then He and Ovaert (2008) developed a 3D contact model between a rough rigid sphere and a semi-infinite anisotropic elastic body, by applying the line integral of Barnett–Lothe tensors (Barnett and Lothe, 1975) on oblique planes. Another method, the Boundary Element Method, is used by Blázquez et al. (2006) for generalized plane problems and by Rodriguez-Tembleque et al. (2011) in 3D to study contact problems in anisotropic solids.

The contact in the layered materials is also an important and interesting subject. Meijers (1968) dealed with the contact problem of a rigid cylinder on an elastic layer. King (1987), King and O'Sullivan (1987), and O'Sullivan and King (1988) looked into the sliding contact on a layered elastic half space. Plumet and Dubourg (1998) investigated the sliding contact between 3D deformable body and multilayered elastic half space. Aizikovich et al. (2002) worked on analytical solutions for a non homogeneous half space. More recently, the anisotropic elastic layer was the subject of many articles. The rigid indenter contact was studied by Batra and Jiang (2008a) with an anisotropic linear elastic layer bonded to a rigid substrate and by Kulchytsky-Zhyhailo and Rogowski (2010) with a layered elastic half space. Kahya et al. (2007) worked on the plane receding contact problem, Batra and Jiang (2008b) studied an analytical solution and Argatov (2011) focused on the depth-sensing indentation. Brock and Georgiadis (2007) presented a class of multiple-zone sliding contact problems, including frictional and thermal effects on an anisotropic half space. Clements and Ang (2009) solved some contact problems for inhomogeneous anisotropic elastic materials and presented contact solution between 3D deformable bodies loaded normally and tangentially against graded layers bonded to heterogeneous substrates.

In a previous study, Bagault et al. (2012) analyzed the effect of anisotropy on the pressure distribution and contact area, when an anisotropic half space is in contact with a rigid sphere. They reduced the formulation given by Pan and Yuan (2000) for an anisotropic bimaterial to the case of an anisotropic half space. A parametric study showed that the stiffness along the normal to the contact has a strong influence on the contact solution in terms of pressure distribution and contact size, whereas a change of the Young's modulus along a direction parallel to the surface does not significantly affect the contact pressure distribution but the contact area is no more circular. The performance of the method is highlighted by analyzing the effect of the orientation of the material main direction compared to the surface normal.

In this paper, starting from three dimensional Green's functions (Yang and Pan, 2002) in anisotropic trimaterials, these functions are derived for layered anisotropic half space, as a sum of infinite space Green's functions and a complementary part, similarly to the Mindlin's superposition method. The Green's functions for anisotropic infinite space have an explicit expression, given by Ting and Lee (1997), whereas the complementary part needs to be integrated numerically.

Several methods can be used for contact simulation of anisotropic materials. Semi analytical methods have proven their efficiency in contact mechanics and are developed here to account for anisotropy of materials. The main advantage is here the small computing time compared to the finite element (FE) method that is however widely used for many contact problems. The contact model between an anisotropic substrate with an anisotropic coating and a rigid sphere will be first presented. Then, the influence of some parameters, as the material properties or the thickness of the layer, on the contact pressure distribution and the contact area shape will be studied.

2. Solution of the contact problem

The semi analytical method (SAM) consists in the summation of elementary solutions known analytically. One of the difficulties is the derivation or the identification of these elementary analytical solutions, such as the well known Boussinesq and Cerruti solutions in isotropic elasticity. The framework of the three dimensional problem is simplified here by assuming the contact between one layered anisotropic elastic half space and a rigid body. The contact area is small in comparison to the dimensions of bodies justifying the assumption of half spaces. Each point of the surface is assigned a value of the pressure corresponding to the total load divided by the surface area. Analytical solutions giving the contributions of normal and tangential loading assumed uniform over a single rectangular element will be used. By summation the elastic deflection at each point within and near the contact area will be derived.

The elastic displacements are expressed by a double discrete convolution product between influence coefficients and the pressure or shear at the contact surface. The normal problem and the tangential problem in partial slip are therefore solved. The solution is performed by minimizing the complementary energy, so the contact pressure is constrained to be positive everywhere and there is no interpenetration. An algorithm is developed based on the conjugated gradient method (CGM). To accelerate the calculation, the fast Fourier transforms (FFT) are used to perform the double convolution product between the pressure and the influence coefficient matrix, at each iteration of the CGM.

Once the contact problem solved, the strains in the coating and in the substrate are calculated.

The semi analytical contact solver is based on the pioneering work of Jacq et al. (2002) for elastic–plastic contacts. The solver has since been developed and improved in several ways. Boucly et al. (2005) and Chen and Wang, 2008 introduced thermal aspects. Fulleringer and Nélias (2010) focused on the influence of a cuboid of uniform plastic strain in a half space, on the normal and tangential displacements of surface points, and derived the corresponding Green's functions in an analytical form. Then Leroux et al. (2010) and Zhou et al. (2011) studied the effects of the presence of inhomogeneous inclusions within a half-space, both on the contact pressure distribution and the subsurface stress field. Discrete convolution (DC) and 3D FFT have been since then widely used in the contact solvers. Leroux and Nélias (2011) worked also on the stick–slip problem for a sphere in contact with a flat half-space containing unidirectional cylindrical fibers. Gallego et al. (2010b) proposed an algorithm based on the conjugate gradient method (CGM) to account for the coupling between normal and tangential effects, which is required for frictional contact problems between elastically dissimilar materials. The same group of researchers also improved the contact algorithm in several ways so that it becomes affordable to simulate wear for 3D contact problems, cycle after cycle (Nélias et al., 2006; Gallego et al., 2006; Gallego and Nélias, 2007). Note that SAM could be also linked with the FE method and used as a zoom on the contact to account for the effect of roughness or simulate wear (Gallego et al., 2010a). More recently Chaise and Nélias (2011) improved the numerical model to account for kinematic and isotropic hardening and analyzed the problem of a rolling load versus indentation. They also proposed a method to predict the coefficient of restitution when an elastic or rigid sphere is impacting an elastic–plastic half-space (Chaise et al., 2011).

3. Influence coefficients for anisotropic layered half space

In the absence of body forces, the equations of equilibrium in terms of displacements u_k are written as $C_{ijkl}u_{k.lj} = 0$. Three matrices 3×3 are defined with the elastic stiffness tensor C_{ijkl} and the vectors n and m, which form a right handed triad with the position vector $x = (x_1, x_2, x_3)^T$. Q, R and T are the double projections of the elastic stiffness tensor.

$$Q_{ik} = C_{ijks} n_j n_s, \quad R_{ik} = C_{ijks} n_j m_s, \quad T_{ik} = C_{ijks} m_j m_s. \tag{1}$$

$$[Q + p_i(R + R^T) + p_i^2 T] a_i = 0. \tag{2}$$

The superscript T denotes transpose of a vector or matrix. Six pairs of eigenvalues p_i and eigenvectors a_i are obtained by solving Eq. (2). Only three pairs of them are independent ($A = (a_1, a_2, a_3)$ and p_i with $Im(p_i) > 0$ and $i = 1, 2, 3$), the three others are their complex conjugates ($\overline{A}$ and $\overline{p}_i$). Matrices $B = (b_1, b_2, b_3)$ and $C = (c_1, c_2, c_3)$ are related to the matrix A by

$$b_i = -\frac{1}{p_i}(Q + p_i R) a_i, \tag{3}$$

with the normalization relation $b_i^T a_j + a_i^T b_j = \delta_{ij}$, and

$$\begin{aligned} &c_i = D_i a_i, \text{ with} \\ &D_{kji} = C_{1kj\alpha} n_\alpha + p_i C_{1kj3} \quad \text{for } k = 1, 2, \\ &D_{3ji} = C_{22j\alpha} n_\alpha + p_i C_{22j3}. \end{aligned} \tag{4}$$

δ_{ij} is the Kronecker delta. The matrix C is different from the fourth-rank elastic stiffness tensor C_{ijkl}, which is always written in its component form in the text. The two matrices M and N are defined by the following expressions.

$$M = BA^{-1}, \quad N = CA^{-1}. \tag{5}$$

The fundamental solution, also called Green's functions, are denoted by $u_{ji}^*(x)$ for the displacement and $\sigma_{jki}^*(x)$ for the stress. The concentrated force f, a vector, is applied at the origin of the reference frame, which is located on the surface of the anisotropic coating ($x_3 \geqslant 0$). The direction of the force is indicated by the last subscript i. Solutions at field point x due to a point force can be written as

$$u_j(x) = u_{ji}^*(x) f_i, \quad \sigma_{jk}(x) = \sigma_{jki}^*(x) f_i. \tag{6}$$

While u is a vector and σ a tensor of second rank, u^* is a tensor of the second rank and σ^* is a tensor of the third rank.

The boundary conditions, at the interface $x_3 = Z_C$, require that the displacement and the traction vector, $t = \sigma(0, 0, 1)^T$, are continuous. Therefore the six stress components are divided in two parts: t^* the traction (out-of-plane stress) vector and s^* the in-plane stress vector. The fundamental stress solutions can be expressed with the derivatives of displacement, taken with respect to the field point x, as

$$\begin{aligned} t^* &\equiv (\sigma_{13i}^*, \sigma_{23i}^*, \sigma_{33i}^*) = (C_{13kl} u_{ki,l}^*, C_{23kl} u_{ki,l}^*, C_{33kl} u_{ki,l}^*), \\ s^* &\equiv (\sigma_{11i}^*, \sigma_{12i}^*, \sigma_{22i}^*) = (C_{11kl} u_{ki,l}^*, C_{12kl} u_{ki,l}^*, C_{22kl} u_{ki,l}^*). \end{aligned} \tag{7}$$

The Green's functions in Fourier transformed domain (denoted by the tilde) can be written in the following series forms,

$$\begin{aligned} \tilde{u}_m^*(x_1, x_2, x_3) &= \tilde{u}_m^{*(\infty)}(x_1, x_2, x_3) + \sum_{n=1}^{\infty} \tilde{u}_m^{*(n)}(x_1, x_2, x_3), \\ \tilde{t}_m^*(x_1, x_2, x_3) &= \tilde{t}_m^{*(\infty)}(x_1, x_2, x_3) + \sum_{n=1}^{\infty} \tilde{t}_m^{*(n)}(x_1, x_2, x_3), \\ \tilde{s}_m^*(x_1, x_2, x_3) &= \tilde{s}_m^{*(\infty)}(x_1, x_2, x_3) + \sum_{n=1}^{\infty} \tilde{s}_m^{*(n)}(x_1, x_2, x_3). \end{aligned} \tag{8}$$

The subscript m defined the material in which the studied point is, 0 for the coating or 2 for the substrate. The infinite part of the displacement and the stress need to be carry out only for the coating, where the concentrated force is applied. In the substrate, this part is equal to zero, as no force is applied. $u_0^{*(\infty)}$, $t_0^{*(\infty)}$, $s_0^{*(\infty)}$ are obtained by Ting and Lee (1997) and the complementary parts by Yang and Pan (2002).

The displacement in the coating, when $0 < x_3 < Z_C$, is decomposed in two parts.

$$\begin{aligned} &\tilde{u}_0^{*(N)}(x_3) = \tilde{u}_{01}^{*(N)}(x_3) + \tilde{u}_{02}^{*(N)}(x_3) \text{ with} \\ &\tilde{u}_{01}^{*(N)}(x_3) = \overline{A}_0 \langle e^{-\overline{ip}_0 \eta x_3} \rangle \overline{A}_0^{-1} \tilde{u}_{01}^{*(N)}(0) \text{ and} \\ &\tilde{u}_{02}^{*(N)}(x_3) = A_0 \langle e^{-ip_0 \eta (x_3 - Z_C)} \rangle A_0^{-1} \tilde{u}_{02}^{*(N)}(Z_C). \end{aligned} \tag{9}$$

According to the value of the order N, first order $N = 1$ or superior order $N = 2, 3, \ldots, \infty$, the displacements in $x_3 = 0$ and $x_3 = Z_C$ have different expressions.

$$\begin{aligned} &\tilde{u}_{01}^{*(1)}(0) = -\overline{M}_0^{-1} M_0 \tilde{u}_0^{*(\infty)}(0), \\ &\tilde{u}_{01}^{*(N)}(0) = -\overline{M}_0^{-1} M_0 \tilde{u}_{02}^{*(N-1)}(0). \end{aligned} \tag{10}$$

$$\begin{aligned} &\tilde{u}_{02}^{*(1)}(Z_C) = (\overline{M}_2 - M_0)^{-1} (\overline{M}_0 - \overline{M}_2) \tilde{u}_0^{*(\infty)}(Z_C), \\ &\tilde{u}_{02}^{*(N)}(Z_C) = (\overline{M}_2 - M_0)^{-1} (\overline{M}_0 - \overline{M}_2) \tilde{u}_{01}^{*(N-1)}(Z_C). \end{aligned} \tag{11}$$

The infinite part of displacement for $x_3 = 0$ and $x_3 = Z_C$ can be written explicitly as

$$\begin{aligned} &\tilde{u}_0^{*(\infty)}(0) = \overline{A}_0 \langle e^{-\overline{ip}_0 \eta 0} \rangle \overline{A}_0^{-1} (M_0 - \overline{M}_0)^{-1}, \\ &\tilde{u}_0^{*(\infty)}(Z_C) = \overline{A}_0 \langle e^{-\overline{ip}_0 \eta Z_C} \rangle \overline{A}_0^{-1} (M_0 - \overline{M}_0)^{-1}. \end{aligned} \tag{12}$$

The stresses are also expressed in two parts and derived expressly from the displacement.

$$\begin{aligned} \tilde{t}_0^{*(N)}(x_3) &= \tilde{t}_{01}^{*(N)}(x_3) + \tilde{t}_{02}^{*(N)}(x_3) = -i\eta \overline{M}_0 \tilde{u}_{01}^{*(N)}(x_3) - i\eta M_0 \tilde{u}_{02}^{*(N)}(x_3), \\ \tilde{s}_0^{*(N)}(x_3) &= \tilde{s}_{01}^{*(N)}(x_3) + \tilde{s}_{02}^{*(N)}(x_3) = -i\eta \overline{N}_0 \tilde{u}_{01}^{*(N)}(x_3) - i\eta N_0 \tilde{u}_{02}^{*(N)}(x_3). \end{aligned} \tag{13}$$

When $x_3 > Z_C$, the studied point is in the substrate. The displacement can be expressed as

$$\tilde{u}_2^{*(N)}(x_3) = \overline{A}_2 \langle e^{-\overline{ip}_2 \eta (x_3 - Z_C)} \rangle \overline{A}_2^{-1} \tilde{u}_2^{*(N)}(Z_C), \tag{14}$$

with, depending on the order N

$$\begin{aligned} &\tilde{u}_2^{*(1)}(Z_C) = (\overline{M}_2 - M_0)^{-1} (\overline{M}_0 - M_0) \tilde{u}_0^{*(\infty)}(Z_C), \\ &\tilde{u}_2^{*(N)}(Z_C) = (\overline{M}_2 - M_0)^{-1} (\overline{M}_0 - M_0) \tilde{u}_{01}^{*(N-1)}(Z_C). \end{aligned} \tag{15}$$

The formulation for the stress is

$$\begin{aligned} &\tilde{t}_2^{*(N)}(x_3) = -i\eta \overline{M}_2 \tilde{u}_2^{*(N)}(x_3), \\ &\tilde{s}_2^{*(N)}(x_3) = -i\eta \overline{N}_2 \tilde{u}_2^{*(N)}(x_3). \end{aligned} \tag{16}$$

The transformed displacement, traction and in-plane stress tensors can be written as a sum of terms with each term having the following form

$$\begin{aligned} \tilde{u}^* &= \tilde{u}^{*(\infty)} + \sum_N i\eta^{-1} J_{N+1} \langle e^{-ir_N \eta} \rangle J_N \cdots \langle e^{-ir_n \eta} \rangle J_n \cdots \langle e^{-ir_0 \eta} \rangle J_0, \\ \tilde{t}^* &= \tilde{t}^{*(\infty)} + \sum_N J_{N+1} \langle e^{-ir_N \eta} \rangle J_N \cdots \langle e^{-ir_n \eta} \rangle J_n \cdots \langle e^{-ir_0 \eta} \rangle J_0, \\ \tilde{s}^* &= \tilde{s}^{*(\infty)} + \sum_N J_{N+1} \langle e^{-ir_N \eta} \rangle J_N \cdots \langle e^{-ir_n \eta} \rangle J_n \cdots \langle e^{-ir_0 \eta} \rangle J_0. \end{aligned} \tag{17}$$

$\tilde{u}^*, \tilde{t}^*$ and $\tilde{s}^*$ do not share necessarily the same vectors r_n and tensors J_n, see Tables 1–3.

By inserting expressions in Eq. (17) into the inverse-transform operator, the displacement u^*, the stresses t^* and s^* are obtained. The in-plane stress s^* has a similar expression than the traction stress t^*.

$$\begin{aligned} u^* &= u^{*(\infty)} + \sum_N \frac{1}{(2\pi)^2} \int_0^\infty \int_0^{2\pi} \eta \tilde{u}^{*(N)} e^{i y_\alpha (X_\alpha - x_\alpha)} d\eta d\theta \\ &= u^{*(\infty)} + \sum_N \frac{1}{(2\pi)^2} \int_0^\infty \int_0^{2\pi} i J_{N+1} \langle e^{-ir_N \eta} \rangle J_N \cdots \langle e^{-ir_n \eta} \rangle J_n \cdots \\ &\quad \langle e^{-ir_0 \eta} \rangle J_0 e^{i y_\alpha (X_\alpha - x_\alpha)} d\eta d\theta \end{aligned} \tag{18}$$

and

Table 1
Coefficients for $\tilde{u}^*_{01}$.

$N=1$	$J_2^{(1)} = \bar{A}_0$	$r_1^{(1)} = \bar{p}_0 x_3$
	$J_1^{(1)} = \bar{A}_0^{-1}(-\bar{M}_0^{-1}M_0)\bar{A}_0$	$r_0^{(1)} = 0$
	$J_0^{(1)} = \bar{A}_0^{-1}(M_0 - \bar{M}_0)^{-1}$	
$N=2$	$J_3^{(2)} = \bar{A}_0$	$r_2^{(2)} = \bar{p}_0 x_3$
	$J_2^{(2)} = \bar{A}_0^{-1}(-\bar{M}_0^{-1}M_0)A_0$	$r_1^{(2)} = -p_0 Z_C$
	$J_1^{(2)} = A_0^{-1}(\bar{M}_2 - M_0)^{-1}(\bar{M}_0 - \bar{M}_2)\bar{A}_0$	$r_0^{(2)} = \bar{p}_0 Z_C$
	$J_0^{(2)} = \bar{A}_0^{-1}(M_0 - \bar{M}_0)^{-1}$	
$N=3$	$J_4^{(3)} = \bar{A}_0$	$r_3^{(3)} = \bar{p}_0 x_3$
	$J_3^{(3)} = \bar{A}_0^{-1}(-\bar{M}_0^{-1}M_0)A_0$	$r_2^{(3)} = -p_0 Z_C$
	$J_2^{(3)} = A_0^{-1}(\bar{M}_2 - M_0)^{-1}(\bar{M}_0 - \bar{M}_2)\bar{A}_0$	$r_1^{(3)} = \bar{p}_0 Z_C$
	$J_1^{(3)} = \bar{A}_0^{-1}(-\bar{M}_0^{-1}M_0)\bar{A}_0$	$r_0^{(3)} = 0$
	$J_0^{(3)} = \bar{A}_0^{-1}(M_0 - \bar{M}_0)^{-1}$	

Table 2
Coefficients for $\tilde{u}^*_{02}$.

$N=1$	$J_2^{(1)} = A_0$	$r_1^{(1)} = p_0(x_3 - Z_C)$
	$J_1^{(1)} = A_0^{-1}(\bar{M}_2 - M_0)^{-1}(\bar{M}_0 - \bar{M}_2)\bar{A}_0$	$r_0^{(1)} = \bar{p}_0 Z_C$
	$J_0^{(1)} = \bar{A}_0^{-1}(M_0 - \bar{M}_0)^{-1}$	
$N=2$	$J_3^{(2)} = A_0$	$r_2^{(2)} = p_0(x_3 - Z_C)$
	$J_2^{(2)} = A_0^{-1}(\bar{M}_2 - M_0)^{-1}(\bar{M}_0 - \bar{M}_2)\bar{A}_0$	$r_1^{(2)} = \bar{p}_0 Z_C$
	$J_1^{(2)} = \bar{A}_0^{-1}(-\bar{M}_0^{-1}M_0)\bar{A}_0$	$r_0^{(2)} = 0$
	$J_0^{(2)} = \bar{A}_0^{-1}(M_0 - \bar{M}_0)^{-1}$	
$N=3$	$J_4^{(3)} = A_0$	$r_3^{(3)} = p_0(x_3 - Z_C)$
	$J_3^{(3)} = A_0^{-1}(\bar{M}_2 - M_0)^{-1}(\bar{M}_0 - \bar{M}_2)\bar{A}_0$	$r_2^{(3)} = \bar{p}_0 Z_C$
	$J_2^{(3)} = \bar{A}_0^{-1}(-\bar{M}_0^{-1}M_0)A_0$	$r_1^{(3)} = -p_0 Z_C$
	$J_1^{(3)} = A_0^{-1}(\bar{M}_2 - M_0)^{-1}(\bar{M}_0 - \bar{M}_2)\bar{A}_0$	$r_0^{(3)} = \bar{p}_0 Z_C$
	$J_0^{(3)} = \bar{A}_0^{-1}(M_0 - \bar{M}_0)^{-1}$	

Table 3
Coefficients for $\tilde{u}^*_2$.

$N=1$	$J_2^{(1)} = \bar{A}_2$	$r_1^{(1)} = \bar{p}_2(x_3 - Z_C)$
	$J_1^{(1)} = \bar{A}_2^{-1}(\bar{M}_2 - M_0)^{-1}(\bar{M}_0 - M_0)\bar{A}_0$	$r_0^{(1)} = \bar{p}_0 Z_C$
	$J_0^{(1)} = \bar{A}_0^{-1}(M_0 - \bar{M}_0)^{-1}$	
$N=2$	$J_3^{(2)} = \bar{A}_2$	$r_2^{(2)} = \bar{p}_2(x_3 - Z_C)$
	$J_2^{(2)} = \bar{A}_2^{-1}(\bar{M}_2 - M_0)^{-1}(\bar{M}_0 - M_0)\bar{A}_0$	$r_1^{(2)} = \bar{p}_0 Z_C$
	$J_1^{(2)} = \bar{A}_0^{-1}(-\bar{M}_0^{-1}M_0)\bar{A}_0$	$r_0^{(2)} = 0$
	$J_0^{(2)} = \bar{A}_0^{-1}(M_0 - \bar{M}_0)^{-1}$	
$N=3$	$J_4^{(3)} = \bar{A}_2$	$r_3^{(3)} = \bar{p}_2(x_3 - Z_C)$
	$J_3^{(3)} = \bar{A}_2^{-1}(\bar{M}_2 - M_0)^{-1}(\bar{M}_0 - M_0)\bar{A}_0$	$r_2^{(3)} = \bar{p}_0 Z_C$
	$J_2^{(3)} = \bar{A}_0^{-1}(-\bar{M}_0^{-1}M_0)A_0$	$r_1^{(3)} = -p_0 Z_C$
	$J_1^{(3)} = A_0^{-1}(\bar{M}_2 - M_0)^{-1}(\bar{M}_0 - \bar{M}_2)\bar{A}_0$	$r_0^{(3)} = \bar{p}_0 Z_C$
	$J_0^{(3)} = \bar{A}_0^{-1}(M_0 - \bar{M}_0)^{-1}$	

$$t^* = t^{*(\infty)} + \sum_N \frac{1}{(2\pi)^2}\int_0^\infty \int_0^{2\pi} \eta \tilde{t}^{*(N)} e^{i y_\alpha (X_\alpha - x_\alpha)} d\eta d\theta$$
$$= t^{*(\infty)} + \sum_N \frac{1}{(2\pi)^2}\int_0^\infty \int_0^{2\pi} \eta J_{N+1}\langle e^{-i r_N \eta}\rangle J_N \cdots \langle e^{-i r_n \eta}\rangle J_n \cdots \langle e^{-i r_0 \eta}\rangle J_0 e^{i y_\alpha (X_\alpha - x_\alpha)} d\eta d\theta. \quad (19)$$

Table 4
Coefficients $G_{ji}^{(N)}$ and $s^{(N)}$.

$N=1$	$G_{ji}^{(1)} = (J_{jk_2})_2^{(1)}(J_{k_2k_1})_1^{(1)}(J_{k_1 i})_0^{(1)}$
	$s^{(1)} = (r_{k_2})_1^{(1)} + (r_{k_1})_0^{(1)} + x_1\cos\theta + x_2\sin\theta$
$N=2$	$G_{ji}^{(2)} = (J_{jk_3})_3^{(2)}(J_{k_3k_2})_2^{(2)}(J_{k_2k_1})_1^{(2)}(J_{k_1 i})_0^{(2)}$
	$s^{(2)} = (r_{k_3})_2^{(2)} + (r_{k_2})_1^{(2)} + (r_{k_1})_0^{(2)} + x_1\cos\theta + x_2\sin\theta$
$N=3$	$G_{ji}^{(3)} = (J_{jk_4})_4^{(3)}(J_{k_4k_3})_3^{(3)}(J_{k_3k_2})_2^{(3)}(J_{k_2k_1})_1^{(3)}(J_{k_1 i})_0^{(3)}$
	$s^{(3)} = (r_{k_4})_3^{(3)} + (r_{k_3})_2^{(3)} + (r_{k_2})_1^{(3)} + (r_{k_1})_0^{(3)} + x_1\cos\theta + x_2\sin\theta$

J_n and r_n are functions of θ but independent of η. As shown in Eq. (17), the transformed displacement and stress are written as the multiplication of a series of exponential functions of η and a factor of η. The double integrals are reducible to a 1D integral by carrying out the integral in η. The reduced integrals are given by

$$u_{ji}^* = u_{ji}^{*(\infty)} + \sum_N \frac{1}{(2\pi)^2}\int_0^{2\pi} G_{ji}^{(N)}\left(\frac{1}{s^{(N)}} + i\delta(s^{(N)})\right)d\theta, \quad (20)$$

$$t_{ji}^* = t_{ji}^{*(\infty)} + \sum_N \frac{1}{(2\pi)^2}\int_0^{2\pi} G_{ji}^{(N)}\left(-\frac{1}{s^{(N)2}} + i\delta'(s^{(N)})\right)d\theta, \quad (21)$$

where $\delta(k)$ is the Dirac delta, and the prime indicates the first derivative with respect to θ, with

$$G_{ji}^{(N)} = (J_{jk_{N+1}})_{N+1}(J_{k_{N+1}k_N})_N \cdots (J_{k_{n+1}k_n})_n \cdots (J_{k_1 i})_0,$$
$$s^{(N)} = (r_{k_{N+1}})_N + \cdots (r_{k_{n+1}})_n + \cdots (r_{k_1})_0 + x_1\cos\theta + x_2\sin\theta. \quad (22)$$

Here, for the contact between a rigid sphere and an anisotropic substrate with a coating, the order N will be limited to $N = 3$, which gives a good approximation (Table 4). Yang and Pan (2002) studied the error for different orders and for this case, the order $N = 4$ does not provide any further significant contribution. This was also numerically verified using the present model. The calculation details are addressed in Appendix A.

4. Application to a layered anisotropic sphere on flat contact

4.1. Validation for an isotropic substrate with an isotropic coating

The first validation is a comparison between the results obtained using the layered anisotropic model when dealing with a layered isotropic half space submitted to an Hertzian loading and the results by O'Sullivan and King (1988). Assuming a rigid indenter, with a spherical tip of radius $R_{indenter}$, in contact with an isotropic half space, the Hertz pressure P_{Hertz} and the Hertz contact radius a_{Hertz} can be written as

$$P_{Hertz} = \frac{3P}{2\pi a_{Hertz}^2}, \quad (23)$$

$$a_{Hertz} = \left(\frac{3PR_{indenter}(1 - v_{solid}^2)}{4E_{solid}}\right)^{(1/3)}. \quad (24)$$

E_S, E_C and v_S, v_C are the Young's modulus and the Poisson's ratio of the isotropic substrate and the isotropic coating, respectively. P represents the load. As in O'Sullivan and King (1988), the indenter radius, $R_{indenter}$, was taken to be 10 times the coating thickness. Materials are assumed cubic, almost isotropic, because isotropic materials lead to double roots which create singularities. The Coulomb's modulus is equal to the isotropic Coulomb's modulus more or less 1%.

The gap between the O'Sullivan solutions and the numerical solutions for the pressure are inferior to 4%, except for the case $E_C = 0.25E_S$ where the difference reaches 6%, see Fig. 1. It can be concluded that the (anisotropic) numerical solution tends towards the (isotropic) analytical solution for isotropic properties, as expected.

4.2. Validation for an anisotropic half space

A finite element model has been developed with the commercial FE package Abaqus (version 6.9), in order to validate the anisotropic semi analytical method; a ball on plane contact is considered.

An isotropic sphere, with Young's modulus 10^6 times larger than the half space Young's modulus and identical Poisson's ratio, is in contact with a semi infinite half space. The mesh is shown in Fig. 2 and described in Table 5. It includes semi infinite elements CIN3D8 on the edges of the body to mimic nil displacements like those obtained within the half space assumption, and quadratic elements with 20 nodes and 27 integration points (C3D20) in the contact area. In order to respect the Hertz conditions, the sphere radius is 30 times larger than the contact radius. To optimize the computation time, properties of symmetry along the direction 1 are used. Nil displacements are imposed at the bottom of the body.

The first step consists in validating the FE mesh through a comparison of the contact solution obtained for an hertzian loading. The error for the pressure distribution (i.e. on the maximum pressure and the contact radius) is smaller than 0.4%.

Then, an anisotropic case is studied. The half space is considered orthotropic, with the same Poisson's ratio and the same Coulomb's modulus. The Young's modulus along direction 3 (the depth) is twice larger than the Young's modulus in directions 1 and 2. In the numerical solution, the coating and the substrate are composed with the same material. The FE and SAM pressure distributions are plotted in Fig. 3. The error for the maximum value of the pressure is lower than 0.2%. A very good agreement is obtained for this case between SAM and FE results.

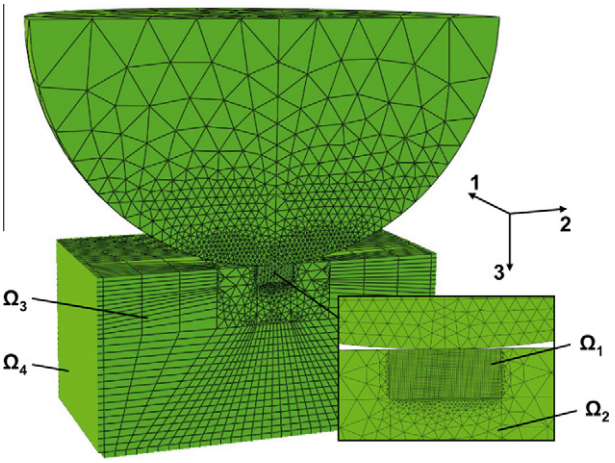

Fig. 2. Finite element model with a detailed view of the contact area.

Table 5
Number and type of elements in the FE model.

Area	*Type*	*Quantity*
Sphere	C3D10	22276
Ω_1	C3D20	54000
Ω_2	C3D4	49656
Ω_3	C3D8R	22942
Ω_4	CIN3D8	3448

4.3. Parametric studies

An elastic anisotropic half space with an anisotropic coating is in contact with a rigid indenter, with a spherical tip. The influence

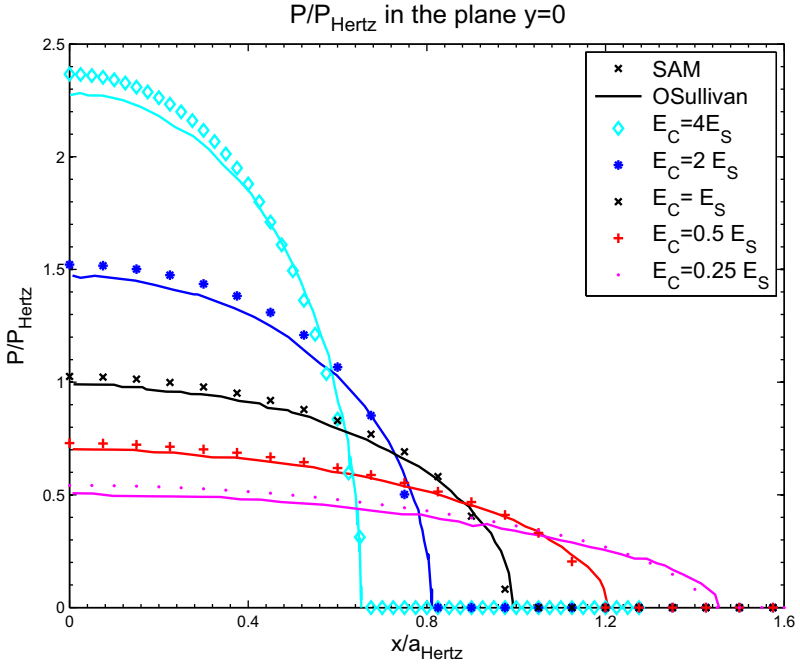

Fig. 1. Pressure profile for layered isotropic case.

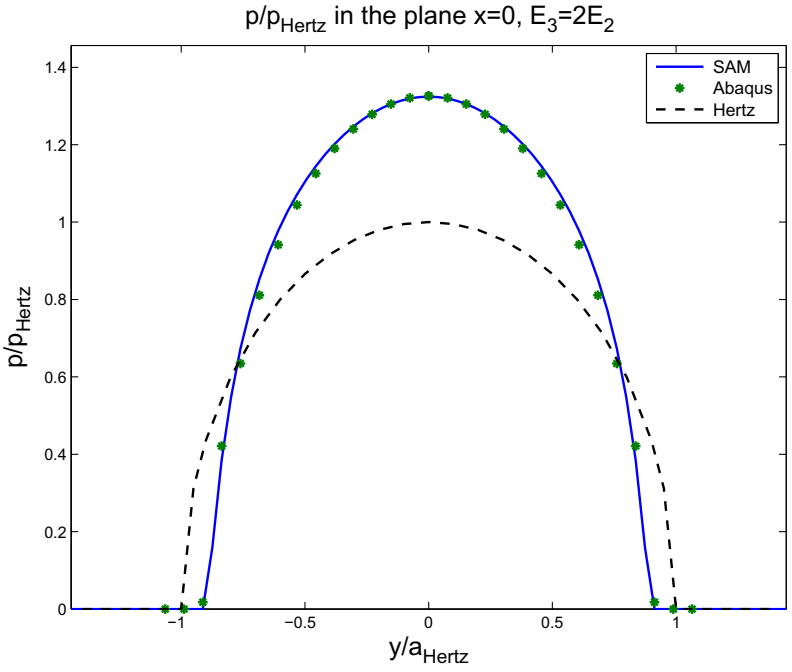

Fig. 3. Dimensionless pressure profile for orthotropic material.

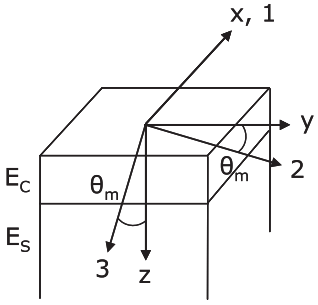

Fig. 4. Coordinate systems.

of the material's properties are studied here. The contact parameters, i.e. the contact area and the pressure distribution, will be more specifically investigated. The depth corresponds to direction 3, which means that the surface is defined by directions 1 and 2. But the material main directions can be different from that of the contact by the angle θ_m (see Fig. 4). (x, y, z) corresponds to the contact reference axes and $(1, 2, 3)$ to the material main direction system. The subscript C represents the coating and S the substrate.

In the first part, materials for the coating are orthotropic and the substrate is cubic, with the same Poisson's ratio and the same Coulomb's modulus. The Coulomb's modulus is slightly modified relative to an isotropic material, in order to avoid singularities. In the second part, roles are reversed, the coating is cubic, almost isotropic, and materials which defined the substrate are orthotropic.

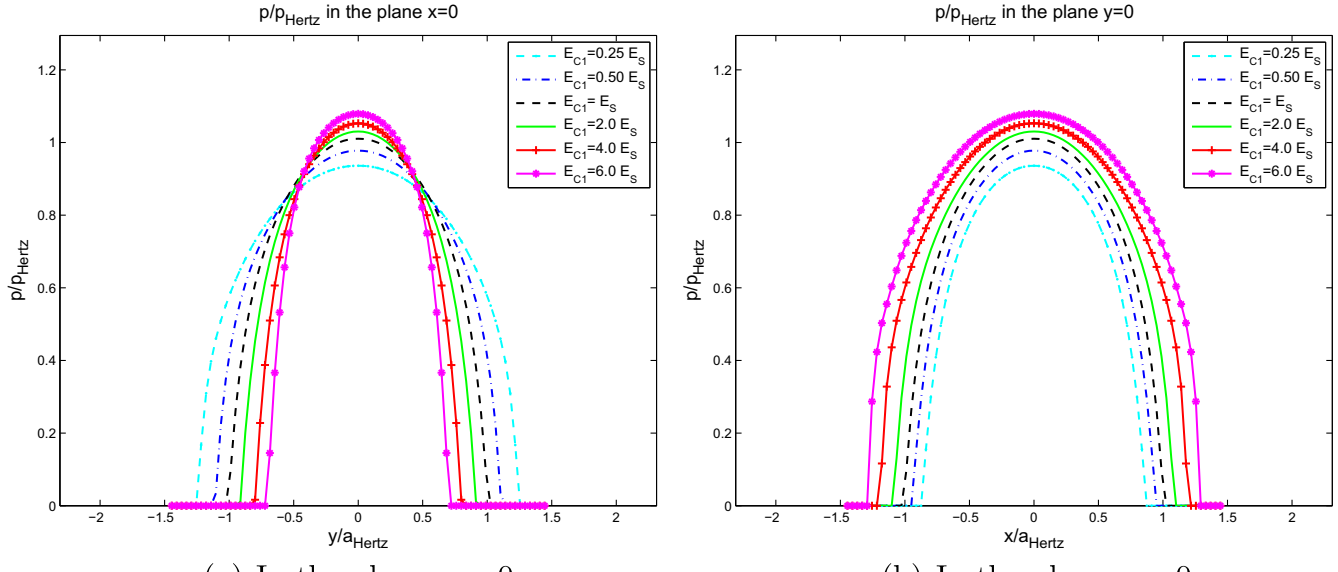

(a) In the plane $x = 0$ (b) In the plane $y = 0$

Fig. 5. Influence of E_{C1} on the contact pressure (isotropic substrate, $Z_C = 0.5a_{Hertz}$).

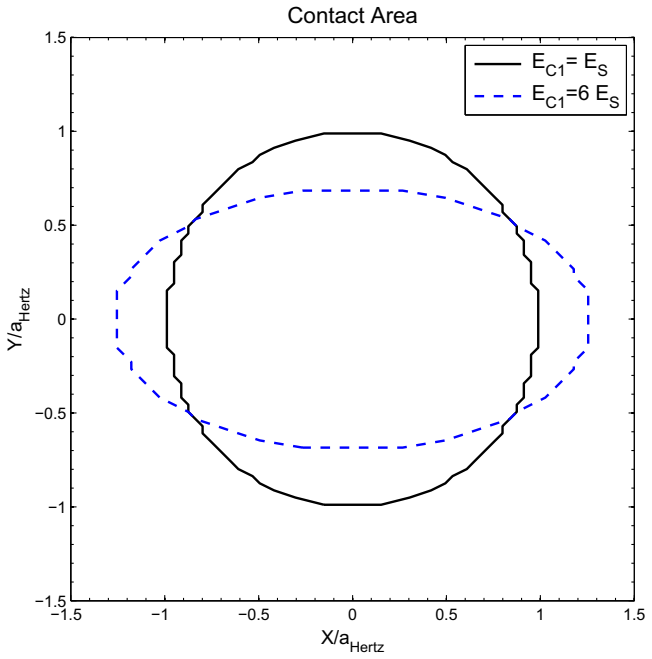

Fig. 6. Influence of E_{C1} on the contact area shape (isotropic substrate, $Z_C = 0.5a_{Hertz}$).

Anisotropic materials are defined by the elastic stiffness tensor C_{ijkl}, which satisfies the full symmetry $C_{ijkl} = C_{jikl} = C_{klij}$. The materials used here are isotropic, cubic (with $G = G_{isotropic} \pm 1\%$) or orthotropic. Depending on these families of materials, two, three or nine parameters are necessary for defining completely the elastic tensor.

4.3.1. An anisotropic coating on an isotropic substrate

The influence of E_{C1} and E_{C3} on the contact pressure distribution is analyzed for E_{C1}/E_S and E_{C3}/E_S ratios ranging from 0.25 to 6 (or 8). Results are plotted in Figs. 5–7. The coating thickness is equal to the half of the Hertz radius, $Z_C = 0.5a_{Hertz}$. It is observed that a change of the coating Young's modulus along a direction parallel to the surface (E_{C1} here) has a limited influence (Fig. 5) on the maximum contact pressure with an increase by 2% when E_{C1} is doubled (and by 6.8% when E_{C1} is multiplied by 6), but has a more pronounced effect on the shape of the contact area. From circular it becomes elliptical (Fig. 6).

The effect of the Young's modulus in the coating along the depth (E_{C3}) is more pronounced: increase of 14% of the maximum contact pressure and decrease of the contact radius by 8% when the Young's modulus is increased by a factor 2 (Fig. 7).

The effect of the material's orientation in the coating relative to the contact can be observed in Fig. 8. The material main directions are different from that of the contact. The maximum pressure is plotted versus the angle, for different ratios between E_{C3} and E_S. When the orientation angle θ_m around the 1-axis increases up to 90°, the numerical solution converges progressively to the solution where the Young's modulus along the depth is equal to the one of the substrate and the one in the surface is different. So the influence of small angles is important because of the effect of the anisotropy along the depth, whereas when the angle increases, the influence decreases since the effect of the Young's modulus along a direction parallel to the surface is moderate. Hence, the method is valid whatever the orientation angle compared to the surface.

Figs. 9 and 10 show the effect of the coating thickness on the contact pressure distribution. In the first one (Fig. 9), the Young's Modulus of the coating in direction 3 is equal to $E_{C3} = 2E_S$. The case $Z_C = 0a_{Hertz}$ corresponds to a half space without coating (an isotropic half space) and the case $Z_C = \infty a_{Hertz}$ to the half space composed only with the coating (an orthotropic half space). When the thickness of the coating increases, the influence of the coating becomes predominant relative to the influence of the substrate as already observed for isotropic layered bodies (Kulchytsky-Zhyhailo and Rogowski, 2010). As $E_{C3} > E_S$, the maximum contact pressure increases with the coating thickness. In the second figure (Fig. 10), the normalized maximum pressure versus the coating thickness is plotted for different E_{C3}/E_S ratios, when the coating is orthotropic (Fig. 10(a)), or different E_C/E_S ratios, when the coating is cubic

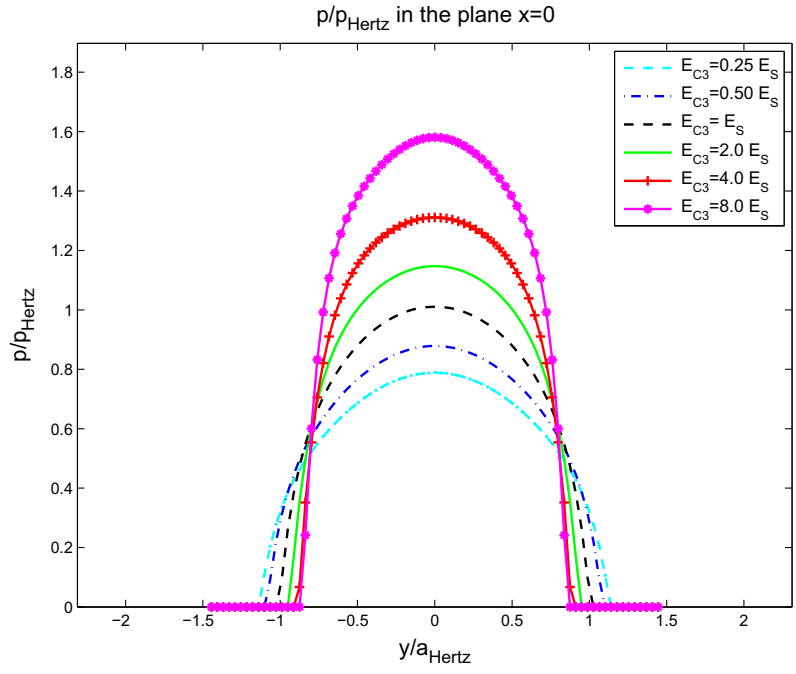

Fig. 7. Influence of E_{C3} on the contact pressure (isotropic substrate, $Z_C = 0.5a_{Hertz}$).

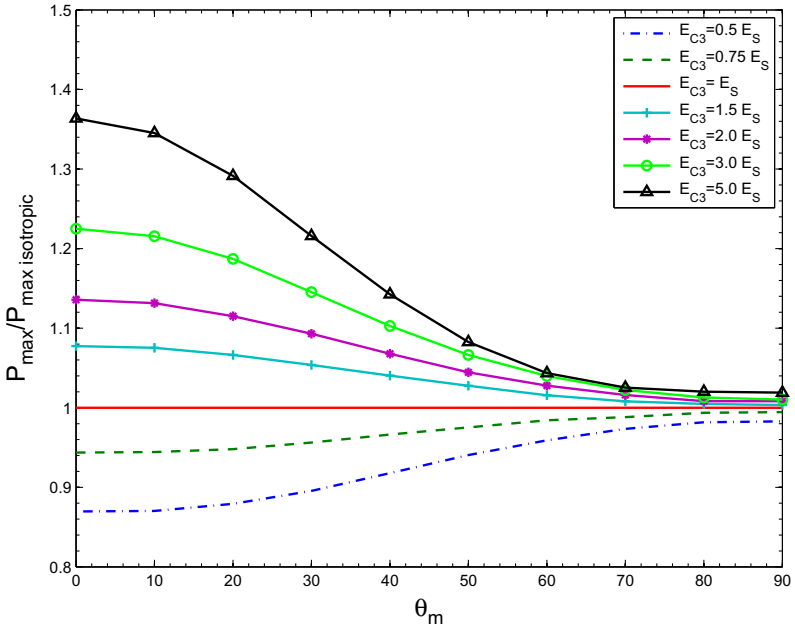

Fig. 8. Influence of the material's orientation on the maximum pressure (isotropic substrate, $Z_C = 0.5a_{Hertz}$).

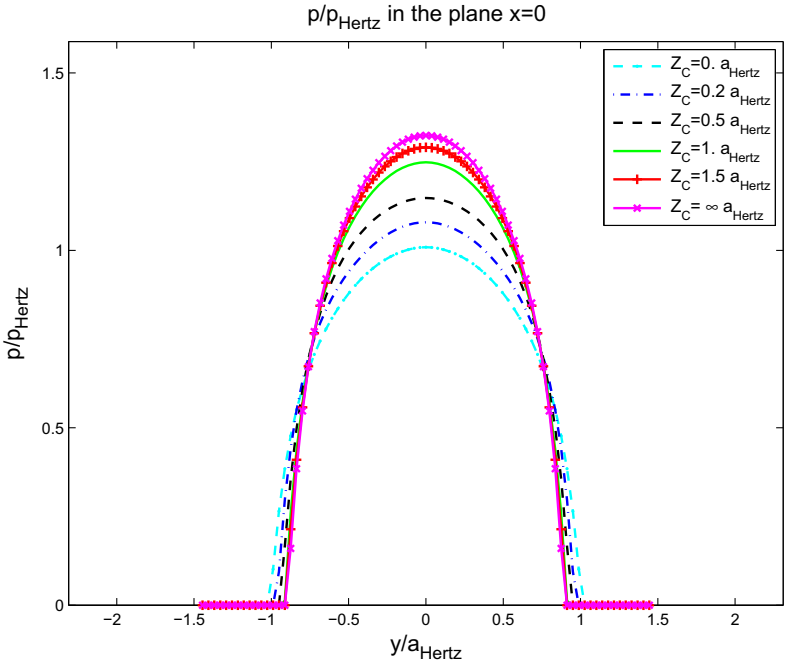

Fig. 9. Influence of Z_C on the contact pressure (isotropic substrate, $E_{C3} = 2E_S$).

almost isotropic (Fig. 10(b)). The maximum pressure increases quickly for small values of Z_C then from $Z_C = a_{Hertz}$ the curve tends slowly to an horizontal asymptote. When the coating is isotropic, the asymptote corresponds to $(E_C/E_S)^{2/3}$. For the case of an orthotropic coating, the asymptote is different but its determination will require further investigations.

4.3.2. An isotropic coating on an anisotropic substrate

The influence of E_{S1} and E_{S3}, the Young's modulus of the substrate, on the contact pressure distribution is investigated here and results summarized in Figs. 11 and 12. The coating thickness is equal to the half of the Hertz radius, $Z_C = 0.5a_{Hertz}$. It can be first observed that the effect of E_{S1} is limited. When E_{S1} is doubled, the maximum pressure increases by 0.7% only. If it is multiplied by 8, the maximum pressure is raised by 3%. Conversely the effect of the Young's modulus of the substrate along the depth, E_{S3}, is more pronounced. The maximum pressure is 13% higher when E_{S3} is twice than $E_{S1} = E_{S2}$. In addition the profile pressure is more rounded when the coating is anisotropic, whereas it is rather domed for the case of an isotropic coating.

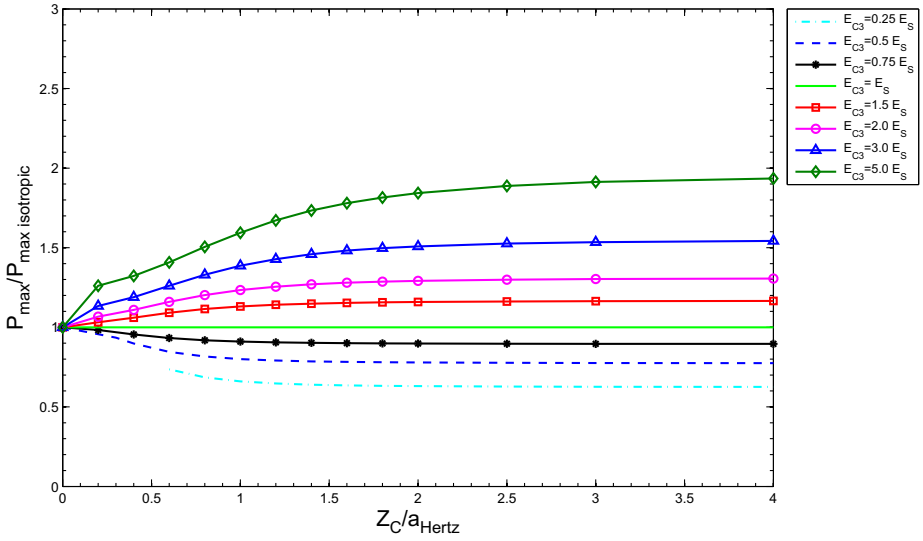

(a) Orthotropic coating

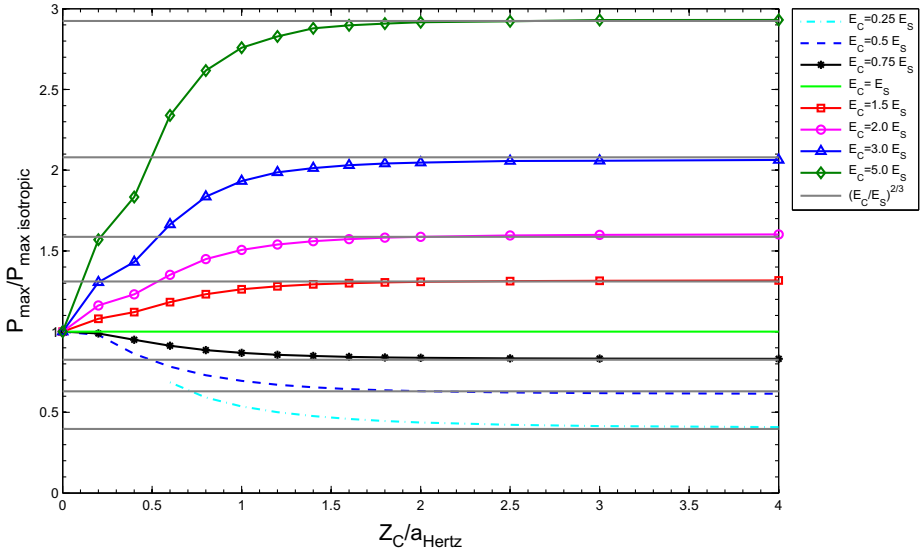

(b) Isotropic coating

Fig. 10. Influence of Z_C on the maximum pressure (isotropic substrate).

Fig. 13 shows the effect of the thickness of an isotropic coating on an anisotropic substrate on the pressure distribution. The Young's modulus of the substrate along direction 3 is twice the one of the coating, $E_{S3} = 2E_C$. When the thickness of the coating increases, the layered half space tends to behave as an isotropic half space. Since here $E_C < E_{S3}$, one may observe a decrease of the maximum contact pressure with the coating thickness. It can be also observed that from $Z_C > 2a_{Hertz}$, the difference between the maximum pressure of the isotropic half space and the layered half space is less than 1%, the coating erases the anisotropy effect of the substrate.

It can be concluded that, for a normal and frictionless contact, the anisotropy along the direction normal to the interface has a strong influence on the contact solution, whether is located the anisotropy, in the coating or in the substrate. Conversely a change of the Young's modulus along a direction parallel to the surface has a limited effect on the maximum contact pressure, however it affects the shape of the contact area that is no longer circular but becomes elliptical. The thickness of the coating changes also the pressure distribution. However this effect vanishes when the coating thickness is higher than the contact radius. Therefore the elastic properties, the direction of anisotropy and the thickness of the coating have to be carefully chosen – and chosen together in a complementary manner – to efficiently protect the substrate.

5. Conclusion

A semi analytical method has been developed for the contact problem of anisotropic elastic materials with an anisotropic coating, by using Green's functions. The model has been validated by

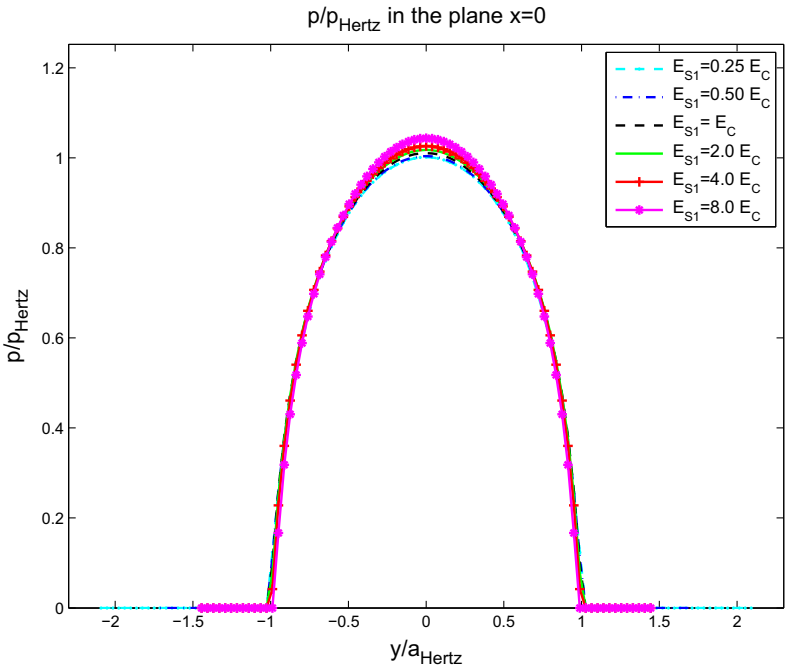

Fig. 11. Influence of E_{S1} on the contact pressure (isotropic coating, $Z_C = 0.5a_{Hertz}$).

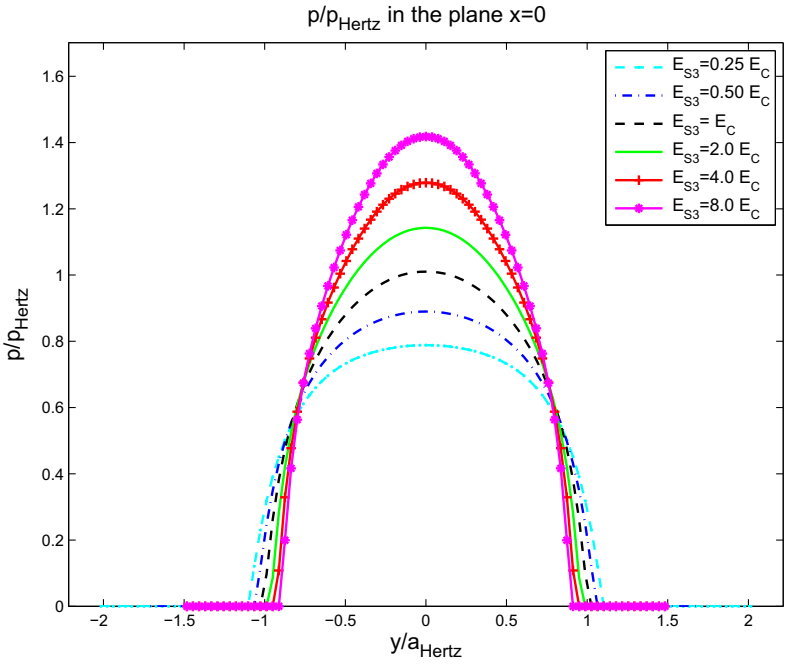

Fig. 12. Influence of E_{S3} on the contact pressure (isotropic coating, $Z_C = 0.5a_{Hertz}$).

comparison with the results of O'Sullivan for isotropic materials with an isotropic coating and by comparison with a FE model for anisotropic half spaces.

A parametric study has been performed for anisotropic coating on an isotropic substrate and for the reversed case, anisotropic substrate with an isotropic coating. It is found that the stiffness along the normal to the contact, in the coating or in the substrate, has a strong influence on the contact solution in terms of pressure distribution and contact size; an increase in E_3, leads to a higher maximum contact pressure and a smaller contact radius. Conversely a change of the Young's modulus along a direction parallel to the surface (plane (1,2)) does not significantly affect the contact pressure distribution, however the contact area is no more circular. The performance of the method is highlighted by analyzing the effect of the orientation of the coating main directions compared to the surface normal. The pressure profile is different, more or less domed, if the anisotropy affects the coating or the substrate. Finally it should be emphasized that, when the coating thickness exceeds the contact radius, the effect of the substrate anisotropy vanishes quickly.

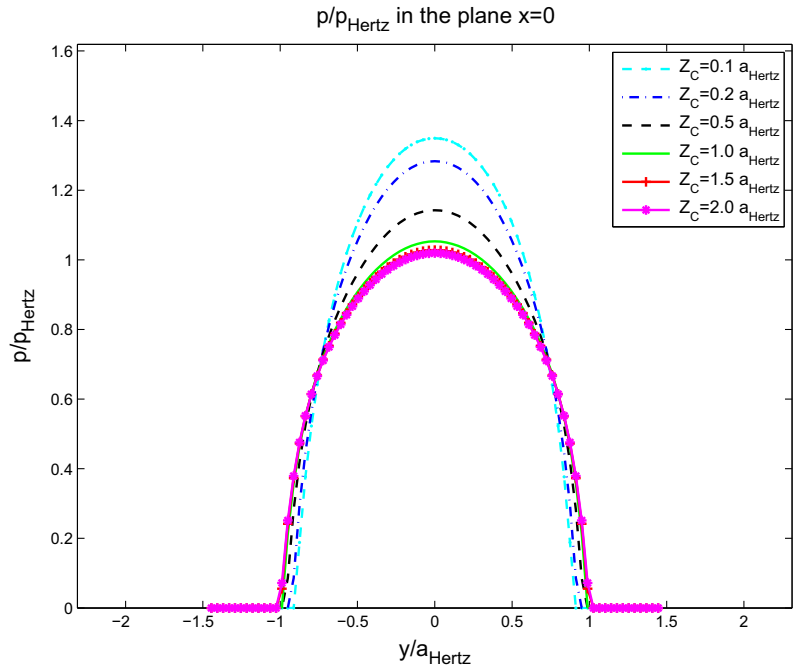

Fig. 13. Influence of Z_C on the contact pressure (isotropic coating, $E_{S3} = 2E_C$).

Acknowledgments

This work was supported by the French FUI Project Innolub. The lead author would like also to gratefully acknowledge the Rhone Alpes Region for providing a doctoral mobility grant.

Appendix A

As discussed in the text, for the case of the contact between a rigid sphere and an anisotropic substrate with a coating, the order N will be limited to $N = 3$.

For $0 < x_3 < Z_C$, Eqs. (20) and (21) are reduced to

$$\begin{aligned}
\tilde{u}_{01}^{*(1)}(x_3) &= i\eta^{-1}\overline{A}_0\langle e^{-i\overline{p}_0\eta x_3}\rangle\overline{A}_0^{-1}(-\overline{M}_0^{-1}M_0)\tilde{u}_0^{*(\infty)}(0)\\
&= i\eta^{-1}\overline{A}_0\langle e^{-i\overline{p}_0\eta x_3}\rangle\overline{A}_0^{-1}(-\overline{M}_0^{-1}M_0)\overline{A}_0\langle e^{-i\overline{p}_0\eta 0}\rangle\\
&\quad\times\overline{A}_0^{-1}(M_0-\overline{M}_0)^{-1},\\
\tilde{u}_{02}^{*(1)}(x_3) &= i\eta^{-1}A_0\langle e^{-ip_0\eta(x_3-Z_C)}\rangle A_0^{-1}(\overline{M}_2-M_0)^{-1}\\
&\quad\times(\overline{M}_0-\overline{M}_2)\tilde{u}_0^{*(\infty)}(Z_C)\\
&= i\eta^{-1}A_0\langle e^{-ip_0\eta(x_3-Z_C)}\rangle A_0^{-1}(\overline{M}_2-M_0)^{-1}\\
&\quad\times(\overline{M}_0-\overline{M}_2)\overline{A}_0\langle e^{-i\overline{p}_0\eta Z_C}\rangle\overline{A}_0^{-1}(M_0-\overline{M}_0)^{-1}.
\end{aligned}\tag{A.1}$$

$$\begin{aligned}
\tilde{u}_{01}^{*(2)}(x_3) &= i\eta^{-1}\overline{A}_0\langle e^{-i\overline{p}_0\eta x_3}\rangle\overline{A}_0^{-1}(-\overline{M}_0^{-1}M_0)\tilde{u}_{02}^{*(1)}(0)\\
&= i\eta^{-1}\overline{A}_0\langle e^{-i\overline{p}_0\eta x_3}\rangle\overline{A}_0^{-1}(-\overline{M}_0^{-1}M_0)A_0\langle e^{-ip_0\eta(-Z_C)}\rangle\\
&\quad\times A_0^{-1}(\overline{M}_2-M_0)^{-1}(\overline{M}_0-\overline{M}_2)\overline{A}_0\langle e^{-i\overline{p}_0\eta Z_C}\rangle\\
&\quad\times\overline{A}_0^{-1}(M_0-\overline{M}_0)^{-1},\\
\tilde{u}_{02}^{*(2)}(x_3) &= i\eta^{-1}A_0\langle e^{-ip_0\eta(x_3-Z_C)}\rangle A_0^{-1}(\overline{M}_2-M_0)^{-1}\\
&\quad\times(\overline{M}_0-\overline{M}_2)\tilde{u}_{01}^{*(1)}(Z_C)\\
&= i\eta^{-1}A_0\langle e^{-ip_0\eta(x_3-Z_C)}\rangle A_0^{-1}(\overline{M}_2-M_0)^{-1}(\overline{M}_0-\overline{M}_2)\\
&\quad\times\overline{A}_0\langle e^{-i\overline{p}_0\eta Z_C}\rangle\overline{A}_0^{-1}(-\overline{M}_0^{-1}M_0)\overline{A}_0\langle e^{-i\overline{p}_0\eta 0}\rangle\\
&\quad\times\overline{A}_0^{-1}(M_0-\overline{M}_0)^{-1}.
\end{aligned}\tag{A.2}$$

$$\begin{aligned}
\tilde{u}_{01}^{*(3)}(x_3) &= i\eta^{-1}\overline{A}_0\langle e^{-i\overline{p}_0\eta x_3}\rangle\overline{A}_0^{-1}(-\overline{M}_0^{-1}M_0)\tilde{u}_{02}^{*(2)}(0)\\
&= i\eta^{-1}\overline{A}_0\langle e^{-i\overline{p}_0\eta x_3}\rangle\overline{A}_0^{-1}(-\overline{M}_0^{-1}M_0)A_0\langle e^{-ip_0\eta(-Z_C)}\rangle\\
&\quad\times A_0^{-1}(\overline{M}_2-M_0)^{-1}(\overline{M}_0-\overline{M}_2)\overline{A}_0\langle e^{-i\overline{p}_0\eta Z_C}\rangle\overline{A}_0^{-1}\\
&\quad\times(-\overline{M}_0^{-1}M_0)\overline{A}_0\langle e^{-i\overline{p}_0\eta 0}\rangle\overline{A}_0^{-1}(M_0-\overline{M}_0)^{-1},\\
\tilde{u}_{02}^{*(3)}(x_3) &= i\eta^{-1}A_0\langle e^{-ip_0\eta(x_3-Z_C)}\rangle A_0^{-1}\\
&\quad\times(\overline{M}_2-M_0)^{-1}(\overline{M}_0-\overline{M}_2)\tilde{u}_{01}^{*(2)}(Z_C)\\
&= i\eta^{-1}A_0\langle e^{-ip_0\eta(x_3-Z_C)}\rangle A_0^{-1}(\overline{M}_2-M_0)^{-1}(\overline{M}_0-\overline{M}_2)\overline{A}_0\\
&\quad\times\langle e^{-i\overline{p}_0\eta Z_C}\rangle\overline{A}_0^{-1}(-\overline{M}_0^{-1}M_0)A_0\langle e^{-ip_0\eta(-Z_C)}\rangle A_0^{-1}(\overline{M}_2-M_0)^{-1}\\
&\quad\times(\overline{M}_0-\overline{M}_2)\overline{A}_0\langle e^{-i\overline{p}_0\eta Z_C}\rangle\overline{A}_0^{-1}(M_0-\overline{M}_0)^{-1}.
\end{aligned}\tag{A.3}$$

$$\begin{aligned}
\tilde{t}_{01}^{*(N)}(x_3) &= -i\eta\overline{M}_0\tilde{u}_{01}^{*(N)}(x_3),\\
\tilde{s}_{01}^{*(N)}(x_3) &= -i\eta\overline{N}_0\tilde{u}_{01}^{*(N)}(x_3).
\end{aligned}\tag{A.4}$$

$$\begin{aligned}
\tilde{t}_{02}^{*(N)}(x_3) &= -i\eta M_0\tilde{u}_{02}^{*(N)}(x_3),\\
\tilde{s}_{02}^{*(N)}(x_3) &= -i\eta N_0\tilde{u}_{02}^{*(N)}(x_3).
\end{aligned}\tag{A.5}$$

For $x_3 > Z_C$, Eqs. (20) and (21) give

$$\begin{aligned}
\tilde{u}_2^{*(1)}(x_3) &= i\eta^{-1}\overline{A}_2\langle e^{-i\overline{p}_2\eta(x_3-Z_C)}\rangle\overline{A}_2^{-1}\tilde{u}_2^{*(1)}(Z_C)\\
&= i\eta^{-1}\overline{A}_2\langle e^{-i\overline{p}_2\eta(x_3-Z_C)}\rangle\overline{A}_2^{-1}(\overline{M}_2-M_0)^{-1}(\overline{M}_0\\
&\quad-M_0)\overline{A}_0\langle e^{-i\overline{p}_0\eta Z_C}\rangle\overline{A}_0^{-1}(M_0-\overline{M}_0)^{-1},
\end{aligned}\tag{A.6}$$

$$\begin{aligned}
\tilde{u}_2^{*(2)}(x_3) &= i\eta^{-1}\overline{A}_2\langle e^{-i\overline{p}_2\eta(x_3-Z_C)}\rangle\overline{A}_2^{-1}\tilde{u}_2^{*(2)}(Z_C)\\
&= i\eta^{-1}\overline{A}_2\langle e^{-i\overline{p}_2\eta(x_3-Z_C)}\rangle\overline{A}_2^{-1}(\overline{M}_2-M_0)^{-1}(\overline{M}_0-M_0)\overline{A}_0\langle e^{-i\overline{p}_0\eta Z_C}\rangle\\
&\quad\times\overline{A}_0^{-1}(-\overline{M}_0^{-1}M_0)\overline{A}_0\langle e^{-i\overline{p}_0\eta 0}\rangle\overline{A}_0^{-1}(M_0-\overline{M}_0)^{-1},
\end{aligned}\tag{A.7}$$

$$\begin{aligned}
\tilde{u}_2^{*(3)}(x_3) &= i\eta^{-1}\overline{A}_2\langle e^{-i\overline{p}_2\eta(x_3-Z_C)}\rangle\overline{A}_2^{-1}\tilde{u}_2^{*(3)}(Z_C)\\
&= i\eta^{-1}\overline{A}_2\langle e^{-i\overline{p}_2\eta(x_3-Z_C)}\rangle\overline{A}_2^{-1}(\overline{M}_2-M_0)^{-1}\\
&\quad\times(\overline{M}_0-M_0)\overline{A}_0\langle e^{-i\overline{p}_0\eta Z_C}\rangle\overline{A}_0^{-1}(-\overline{M}_0^{-1}M_0)A_0\langle e^{-ip_0\eta(-Z_C)}\rangle A_0^{-1}\\
&\quad\times(\overline{M}_2-M_0)^{-1}(\overline{M}_0-\overline{M}_2)\overline{A}_0\langle e^{-i\overline{p}_0\eta Z_C}\rangle\overline{A}_0^{-1}(M_0-\overline{M}_0)^{-1}.
\end{aligned}\tag{A.8}$$

$$\begin{aligned}
\tilde{t}_2^{*(N)}(x_3) &= -i\eta\overline{M}_2\tilde{u}_2^{*(N)}(x_3),\\
\tilde{s}_2^{*(N)}(x_3) &= -i\eta\overline{N}_2\tilde{u}_2^{*(N)}(x_3).
\end{aligned}\tag{A.9}$$

References

Aizikovich, S., Alexandrov, V., Kalker, J., Krenev, L., Trubchik, I., 2002. Analytical solution of the spherical indentation problem for a half-space with gradients with the depth elastic properties. International Journal of Solids and Structures 39 (10), 2745–2772.

Argatov, I., 2011. Depth-sensing indentation of a transversely isotropic elastic layer: second-order asymptotic models for canonical indenters. International Journal of Solids and Structures 48 (25–26), 3444–3452.

Bagault, C., Nelias, D., Baietto, M.-C., 2012. Contact analyses for anisotropic half space: effect of the anisotropy on the pressure distribution and contact area. Journal of Tribology 134 (3), 031401-1–031401-8.

Barnett, D., Lothe, J., 1975. Line force loadings on anisotropic half-spaces and wedges. Physica Norvegica 8 (1), 13–22.

Batra, R., Jiang, W., 2008a. Analytical solution of the contact problem of a rigid indenter and an anisotropic linear elastic layer. International Journal of Solids and Structures 45 (22–23), 5814–5830.

Batra, R., Jiang, W., 2008b. Analytical solution of the contact problem of a rigid indenter and an anisotropic linear elastic layer. International Journal of Solids and Structures 45 (22), 5814–5830.

Blázquez, A., Mantič, V., Par's, F., 2006. Application of BEM to generalized plane problems for anisotropic elastic materials in presence of contact. Engineering Analysis with Boundary Elements 30 (6), 489–502.

Borodich, F., 2000. Some contact problems of anisotropic elastodynamics: integral characteristics and exact solutions. International Journal of Solids and Structures 37 (24), 3345–3373.

Boucly, V., Nelias, D., Liu, S., Wang, Q., Keer, L., 2005. Contact analyses for bodies with frictional heating and plastic behavior. Journal of Tribology 127 (2), 355–364.

Boussinesq, J., 1885. Application des Potentiels à l'Étude de l'Équilibre et du Mouvement des Solides Élastiques. Gauthier-Villars.

Brock, L., Georgiadis, H., 2007. Multiple-zone sliding contact with friction on an anisotropic thermoelastic half-space. International Journal of Solids and Structures 44 (9), 2820–2836.

Chaise, T., Nélias, D., 2011. Contact pressure and residual strain in 3d elasto-plastic rolling contact for a circular or elliptical point contact. Journal of Tribology 133 (4), 041402-1–041402-9.

Chaise, T., Nélias, D., Sadeghi, F., 2011. On the effect of isotropic hardening on the coefficient of restitution for single or repeated impacts using a semi-analytical method. Tribology Transactions 54 (5), 714–722.

Chen, W., Wang, Q., 2008. Thermomechanical analysis of elastoplastic bodies in a sliding spherical contact and the effects of sliding speed, heat partition, and thermal softening. Journal of Tribology 130 (4), 041402-1–041402-10.

Ciavarella, M., Demelio, G., Schino, M., Vlassak, J., 2001. The general 3d hertzian contact problem for anisotropic materials. Key Engineering Materials 221, 281–292.

Clements, D., Ang, W., 2009. On some contact problems for inhomogeneous anisotropic elastic materials. International Journal of Engineering Science 47 (11–12), 1149–1162.

Fulleringer, B., Nélias, D., 2010. On the tangential displacement of a surface point due to a cuboid of uniform plastic strain in a half-space. Journal of Applied Mechanics 77 (2), 021014-1–021014-7.

Galin, L., 2008. Contact Problems: The Legacy of LA Galin. Springer Verlag.

Gallego, L., Fulleringer, B., Deyber, S., Nelias, D., 2010a. Multiscale computation of fretting wear at the blade/disk interface. Tribology International 43 (4), 708–718.

Gallego, L., Nélias, D., 2007. Modeling of fretting wear under gross slip and partial slip conditions. Journal of Tribology 129 (3), 528–535.

Gallego, L., Nelias, D., Deyber, S., 2010b. A fast and efficient contact algorithm for fretting problems applied to fretting modes i, ii and iii. Wear 268 (1–2), 208–222.

Gallego, L., Nélias, D., Jacq, C., 2006. A comprehensive method to predict wear and to define the optimum geometry of fretting surfaces. Journal of Tribology 128 (3), 476–485.

Gao, Y., Pharr, G., 2007. Multidimensional contact moduli of elastically anisotropic solids. Scripta Materialia 57 (1), 13–16.

He, L., Ovaert, T., 2008. Three-dimensional rough surface contact model for anisotropic materials. Journal of Tribology 130 (2), 021402-1–021402-6.

Jacq, C., Nélias, D., Lormand, G., Girodin, D., 2002. Development of a three-dimensional semi-analytical elastic–plastic contact code. Journal of Tribology 124 (4), 653–667.

Kahya, V., Ozsahin, T., Birinci, A., Erdol, R., 2007. A receding contact problem for an anisotropic elastic medium consisting of a layer and a half plane. International Journal of Solids and Structures 44 (17), 5695–5710.

Kelvin, L., 1848. Note on the integration of the equations of equilibrium of an elastic solid. Cambridge and Dublin Mathematical Journal 3, 87–89.

King, R., 1987. Elastic analysis of some punch problems for a layered medium. International Journal of Solids and Structures 23 (12), 1657–1664.

King, R., O'Sullivan, T., 1987. Sliding contact stresses in a two-dimensional layered elastic half-space. International Journal of Solids and Structures 23 (5), 581–597.

Kulchytsky-Zhyhailo, R., Rogowski, G., 2010. Stresses in hard coating due to a rigid spherical indenter on a layered elastic half-space. Tribology International 43 (9), 1592–1601.

Leroux, J., Fulleringer, B., Nelias, D., 2010. Contact analysis in presence of spherical inhomogeneities within a half-space. International Journal of Solids and Structures 47 (22–23), 3034–3049.

Leroux, J., Nélias, D., 2011. Stick–slip analysis of a circular point contact between a rigid sphere and a flat unidirectional composite with cylindrical fibers. International Journal of Solids and Structures 48 (25–26), 3510–3520.

Li, X., Wang, M., 2006. Hertzian contact of anisotropic piezoelectric bodies. Journal of Elasticity 84 (2), 153–166.

Lin, Y., Ovaert, T., 2004. A rough surface contact model for general anisotropic materials. Journal of Tribology 126 (1), 41–49.

Meijers, P., 1968. The contact problem of a rigid cylinder on an elastic layer. Applied Scientific Research 18 (1), 353–383.

Mindlin, R., 1936. Force at a point in the interior of a semi-infinite solid. Physics 7 (5), 195–202.

Nélias, D., Boucly, V., Brunet, M., 2006. Elastic-plastic contact between rough surfaces: proposal for a wear or running-in model. Journal of Tribology 128 (2), 236–244.

O'Sullivan, T., King, R., 1988. Sliding contact stress field due to a spherical indenter on a layered elastic half-space. Journal of Tribology 110 (2), 235–240.

Pagano, N., 1970. Exact solutions for rectangular bidirectional composites and sandwich plates. Journal of Composite Materials 4 (1), 20–34.

Pan, E., Yang, B., 2003. Three-dimensional interfacial Green's functions in anisotropic bimaterials. Applied Mathematical Modelling 27 (4), 307–326.

Pan, E., Yuan, F., 2000. Three-dimensional Green's functions in anisotropic bimaterials. International Journal of Solids and Structures 37 (38), 5329–5351.

Plumet, S., Dubourg, M.-C., 1998. A 3-d model for a multilayered body loaded normally and tangentially against a rigid body: application to specific coatings. Journal of Tribology 120 (4), 668–676.

Rand, O., Rovenskii, V., 2005. Analytical Methods in Anisotropic Elasticity: With Symbolic Computational Tools. Birkhauser.

Rodriguez-Tembleque, L., Buroni, F., Abascal, R., Sáez, A., 2011. 3d frictional contact of anisotropic solids using BEM. European Journal of Mechanics-A/Solids 30 (2), 95–104.

Stroh, A., 1958. Dislocations and cracks in anisotropic elasticity. Philosophical Magazine 3 (30), 625–646.

Stroh, A., 1962. Steady state problems in anisotropic elasticity. Journal of Mathematical Physics 41 (2), 77–103.

Swanson, S., 2004. Hertzian contact of orthotropic materials. International Journal of Solids and Structures 41, 1945–1959.

Ting, T., 1996. Anisotropic Elasticity: Theory and Applications. Oxford University Press, USA.

Ting, T., Lee, V., 1997. The three-dimensional elastostatic Green's function for general anisotropic linear elastic solids. The Quarterly Journal of Mechanics and Applied Mathematics 50 (3), 407–426.

Willis, J., 1966. Hertzian contact of anisotropic bodies. Journal of the Mechanics and Physics of Solids 14 (3), 163–176.

Yang, B., Pan, E., 2002. Three-dimensional Green's functions in anisotropic trimaterials. International Journal of Solids and Structures 39 (8), 2235–2255.

Zhou, K., Keer, L., Wang, Q., 2011. Semi-analytic solution for multiple interacting three-dimensional inhomogeneous inclusions of arbitrary shape in an infinite space. International Journal for Numerical Methods in Engineering 87 (7), 617–638.